*Geotechnical Aspects of Underground Construction in Soft Ground – Ng, Huang & Liu (eds)*


# Two distinctive shear strain modes for pile-soil-tunnelling interaction in a granular mass

Y.J. Lee
*Soil-Structure Interaction Group, Steel Structure Research Laboratory, Research Institute of Industrial Science & Technology (RIST), South Korea*

C.S. Yoo
*Department of Civil & Environmental Engineering, Sungkyunkwan University, South Korea*

ABSTRACT: There are many high-rise buildings in urban areas, which are normally supported by piled foundations. Consequently, a major concern for geotechnical engineers is the construction of a tunnel adjacent to the piled foundations, since ground behaviour between an existing loaded pile and tunnelling has not been understood well so far, particularly for granular soils rather than clay soils. In order to figure out such complicated ground behaviour, the interactive shear strain patterns are generated by two-dimensional laboratory model tests and finite element analyses (FEA). For the model testing, a multi-sized aluminium rod mixture considered as a continuum granular mass and close range photogrammetric technique for obtaining displacement data within the rods are introduced. Two distinctive shear strain modes, viz. connective and isolated modes, are presented through the comparison of the model tests and FEA according to the pile tip locations.

## 1 INTRODUCTION

Tunnel excavation work in the soft ground results in significant reduction in total stress in the vicinity of a tunnel boundary. The reduction in stress causes ground movements which affect adjacent building foundations consisted of a row of loaded piles.

In order to identify the pile-soil-tunnelling interaction behaviour, small-scale physical model tests and numerical methods were employed in this study. Careful assessment of the pile-soil-tunnelling interaction problems is relatively new and only limited information is currently available.

This study focuses on two distinctive shear strain modes of the ground between the existing pile and a new tunnel construction as shown in Figure 1. The laboratory model tests were conducted by strain control rather than stress control, and then comparison with the finite element analyses was carried out to identify the shear strain modes. This research incorporates strain controlled tests with idealised two-dimensional aluminium rods – considered as a granular mass – taken to very high volume loss (up to about 20%) to highlight the full shear failure formation. Digital image processing technique has allowed overall deformation patterns of ground movements to be obtained from the analysis of digital images. Detailed shear strain patterns of the ground can be obtained which give a clear insight into the pile-soil-tunnelling interaction events.

The model pile was principally an end-bearing pile where most of the pile load is concentrated on the pile tip rather than pile shaft. The pile working load was maintained constant during the test. This working load was chosen by reference to a displacement-controlled pile-load test (the pile working load, 3.6 kN, is 77% of the ultimate pile load). In this study, in order to avoid complexity of pile loading the influence of lateral loading was not considered.

## 2 LABORATORY MODEL TEST

### 2.1 *Test equipment*

The displacement-controlled model tunnel consists of 6 segments, the two ends of a segment being carved on tapered cones. Each segment moves inward as the tapers are withdrawn, simulating the two-dimensional volume loss during tunnelling operations. The tunnel diameter is reduced by rotating the two knobs as shown in Figure 2. The outer diameter of the tunnel is initially 100 mm. The reduction of the tunnel diameter gives directly a 2D volume loss ($V_L$). This 2D volume loss per revolution is determined from the calibration result (Lee, 2004).

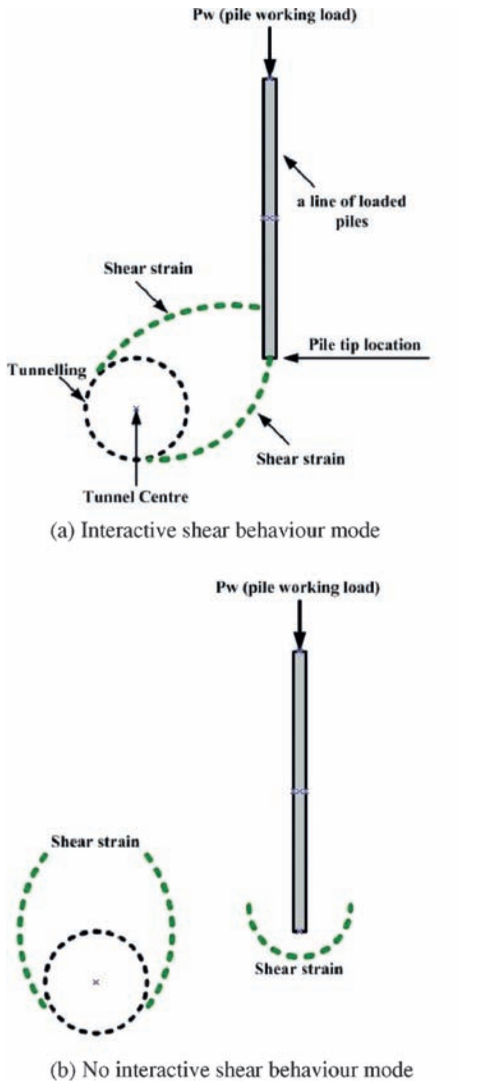


Figure 1. Schematic illustration of shear strain modes for the pile-soil-tunnelling interaction.

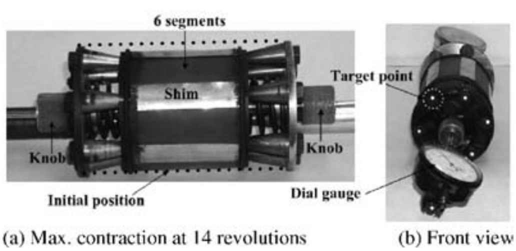


Figure 2. Diameter reduction system of model tunnel.

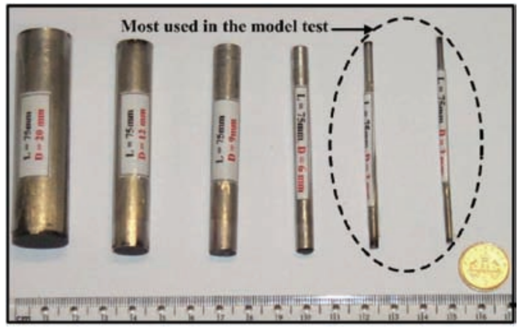


Figure 3. Multi-sized aluminium rod material.

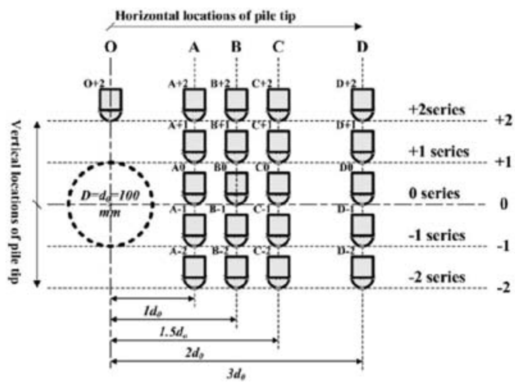


Figure 4. Identification of pile tip location.

The aluminium rod mixture consists of six different diameters (viz. 2 mm, 3 mm, 6 mm, 9 mm, 12 mm and 20 mm), which have the same length of 75 mm. It represents a well graded, idealised two-dimensional granular material, as shown in Figure 3. The test chamber is rigid, a rectangular steel frame (width: 1058 mm, height: 930 mm). The model pile (25 mm $\times$ 75 mm in cross section, embedded length, L: 370 mm) is made of aluminium alloy. No significant effects of the boundary conditions were observed during the test, since the smallest rods (2 mm and 3 mm diameters) were mainly used in the interactive regions and the largest rods were used in the vicinity of the steel frame boundaries.

### 2.2 *Pile-soil-tunnelling interaction test*

The pile tip identification system adopted was to label the distances of the pile tip away from the tunnel centre line (O) as A ($1d_0$: model tunnel diameter), B ($1.5d_0$), C ($2d_0$), D ($3d_0$) and the pile tip level as 0 (on the centre line), $+1$ (on the crown level), $+2$ (at $1d_0$ above the centre line level), $-1$ and $-2$ being similarly below the centre line level. One final location ($O + 2$) was with the pile directly above the centre line of the tunnel on the $+2$ level (Figure 4).

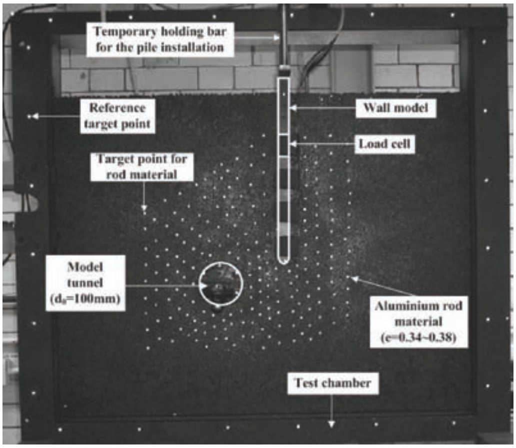


Figure 5. Set-up stage with test equipment and reflective target points.

The pile was in place and loaded before any of the pile-soil-tunnelling interaction occurred. The model tests, therefore, simulated new tunnelling adjacent to a row of existing loaded piles.

Each model test normally consisted of three stages as follows: (1) set-up stage, material 'compacted' as before, with reflective nodes shown in Figure 5 (both pile and tunnel installed in positions but with no pile loading and tunnel at initial diameter, $d_0$); (2) pile loaded to working load by dead weight ($P_w$ from the pile-load test); (3) tunnelling stage (reduction of the tunnel diameter to a maximum value of 12 revolutions, i.e. $V_L = 18.65\%$).

The tests using aluminium rods in this study are much quicker to carry out in terms of testing time than any conventional test using a real soil such as sand or clay. In addition, detailed observation of the side section can easily be carried out, enabling details of the failure mechanisms, which are associated with strain fields rather than stress fields, to be examined.

## 3 CLOSE RANGE PHOTOGRAMMETRY

The close range photogrammetric technique for determining strains used in this study has recently been applied to a number of geotechnical engineering problems. A Kodak DC 290 digital camera was used to capture both the frame (or chamber) reference points and the target points fixed to the centre part at the ends of the smaller size rods within the multi-sized rod matrix. The digital camera can provide acceptably high resolution. Ten independent images were taken at each epoch (or stage) using the Kodak DC 290 digital camera as shown in Figure 6.

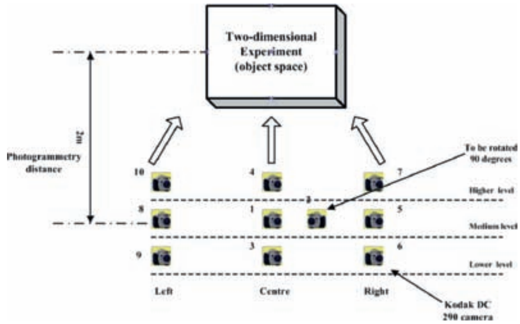


Figure 6. Typical digital camera positions for capturing 10 images.

A pixel resolution of $1792 \times 1200$ was available. Each retro-reflective target was identified and the position of its image within each of the ten photographs was measured by the VMS (vision metrology system) program. The measured 2D x-y coordinates of the target points from the VMS are arranged into a triangulation mesh by means of the EngVis program. Figure 7 shows an example of the imaging processing by the VMS and the subsequent triangulation by the EngVis respectively.

The system and its application were described by Woodhouse et al. (1999), Woodhouse (2000) and Kwok and Swajani (2001). From the measured displacements, strains were calculated based on the assumption of linear strain in each triangular element (Lee and Bassett, 2006). More detailed model test procedures matched with the image capturing stages are shown in Figure 8.

## 4 NUMERICAL ANALYSIS

In order to carry out the finite element analyses (FEA), the 3D pile-soil-tunnelling interaction situation was idealised to two-dimensional plane-strain conditions and to compare with the model pile-soil-tunnelling test result, the same tunnel geometry, pile size, and location of the pile relative to the tunnel were adopted for the FEA. The FE analyses were carried out using the continuum finite element program CRISP (Britto and Gunn, 1987; Woods and Rahim, 2001).

Ground behaviour was assumed to be governed by an elastic-perfectly-plastic constitutive model based on the Mohr-Coulomb failure criterion with a non-associated flow rule. The critical state angle of friction ($\phi'_{cs}$) and the angle of dilation ($\psi$) were determined to be 23° and 15° for the model granular material, respectively (based on a best FEA fit of load-settlement relationship for the model pile loading tests, Lee, 2004). It should be noted that later these parameters were also obtained from shear box tests (area void

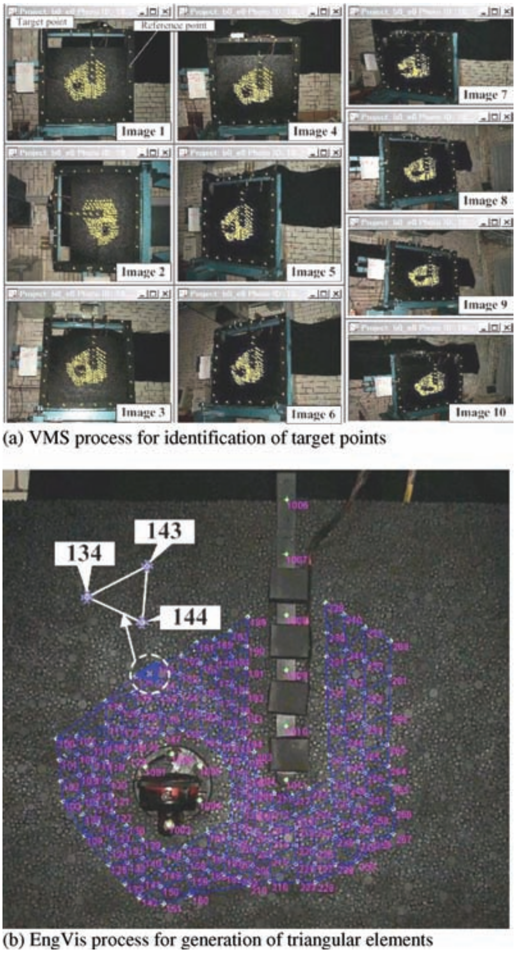


(a) VMS process for identification of target points

(b) EngVis process for generation of triangular elements

Figure 7. Digital image analysis by VMS and EngVis programs.

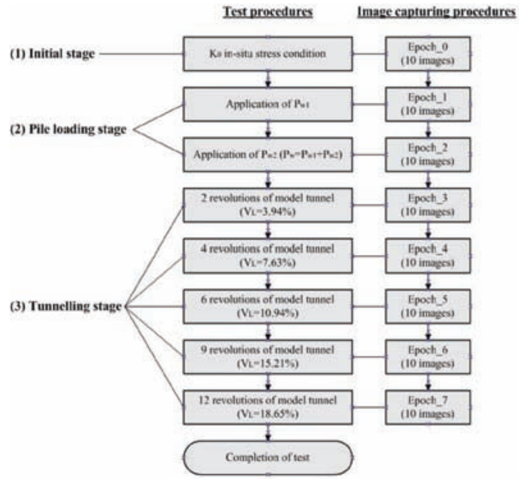


Figure 8. Relationship between model test steps and image capturing stages.

Table 1. Ground parameters used in the FEA.

| | |
|---|---|
| Ground surface level, $Y_0^*$(m) | 0.72 |
| Young's modulus at $Y_0$, $E_0^*$(kPa) | 1600 |
| Gradient of Young's modulus, $m_E^{**}$(kPa/m) | 10,000 |
| Poisson's ratio, $\nu$ | 0.35 |
| Unit weight of soil, $\gamma$ (kN/m$^3$) | 24 |
| Effective cohesion, c′ (kPa) | 0.1 |
| Critical state angle of friction, $\phi'_{cs}$ (degrees) | 23 |
| Angle of dilation, $\psi$ (degrees) | 15 |

Note: *from bottom to top of mesh; **varying with depth

Table 2. Parameters for tunnel support and pile.

| Parameters | Tunnel support | Pile |
|---|---|---|
| $E$ (GPa) | 15.5 | 15.5 |
| $\nu$ | 0.2 | 0.2 |
| Unit weight, $\gamma$ (kN/m$^3$) | – | 23 |
| Cross section area, A (m$^2$) | 0.003 | – |

ratio, e = 0.34 ~ 0.38, $\phi'_{cs}$ and e values are found to be similar to those given by Yamamoto and Kusuda, 2001). Parameter values from the shear box tests were comparable to the best fit values. The effective cohesion (c′) was assumed to be 0.1 kPa. The variation of Young's modulus (E) was assumed to increase linearly with depth. The ground parameters are summarised in Table 1.

The tunnel support and pile was modelled as a two-node bar element and linear elastic material respectively. The Young's modulus and Poisson's ratio for both the tunnel support and pile were assumed to be 15.5 GPa and 0.2, respectively. The unit weight of the pile and the cross section area of the tunnel support ring were 23 kN/m$^3$ and 0.003 m$^2$, respectively. The model parameters for the tunnel support and the pile are summarised in Table 2.

FNR (Full Newton-Raphson) iterative solution scheme was adopted together with a tolerance of 0.05 and a maximum iteration number of 100. $K_0$ (0.66) was applied as the initial in-situ stress conditions. Double convergence check based on both the displacement and force norms and a total of 1055 increments were used. It should be noted that the largest 2D volume loss values (7.63% to 18.65%) were generated in order to capture the interaction failure patterns between the pile and the tunnel.

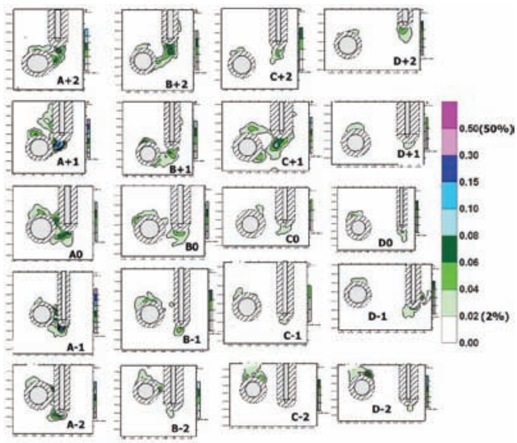


(a) Model Tests

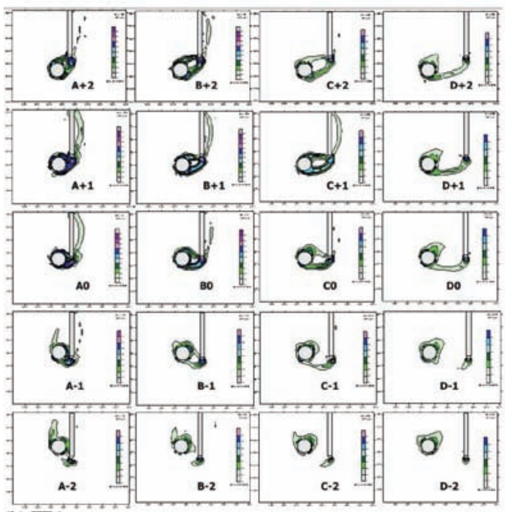

(b) FEA

Figure 9. Comparison of maximum shear strain contours at $V_L = 3.94\%$.

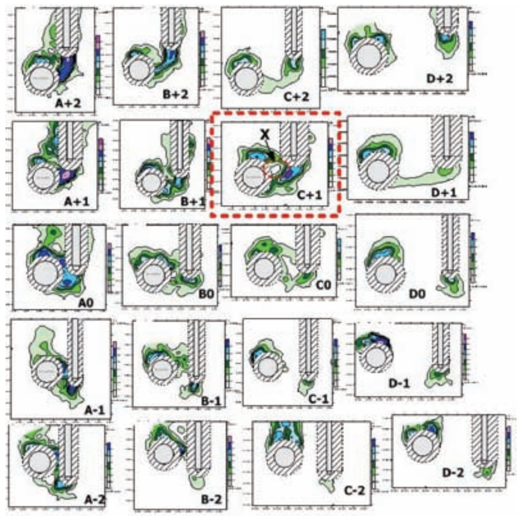


(a) Model Tests

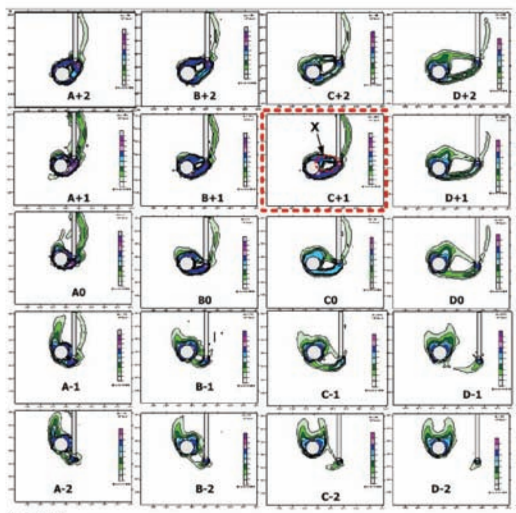


(b) FEA

Figure 10. Comparison of maximum shear strain contours at $V_L = 10.94\%$.

## 5 RESULTS

Figures 9 and 10 show the maximum shear strain contours of the model tests at $V_L = 3.94\%$ and $V_L = 10.94\%$ respectively. The location and intensity of shear strain clearly identify the developing shear failure formation between the pile base and the tunnel. It is noted that the case of O + 2 was omitted in this comparison (this case is not a normal practice for considering a proper tunnel position adjacent to a row of loaded piles).

A clear neutral or dead block X – an area with low or no strain – was observed clearly in case C + 1 at 10.94% of volume loss as shown in Figure 10.

The shear failure formation appeared to comprise two distinctive shear strain modes: (1) one that includes a "neutral soil block" X, separating a formation running from the pile base to the tunnel invert area and a second mechanism running from the pile shaft to the tunnel crown area, and (2) the other one that is an independent shear behaviour mode, i.e. no interactive shear strain mode between the pile and the tunnel. In summary, the two different shear strain modes shown in Figure 1 can be identified according to pile tip locations as shown in Figure 11.

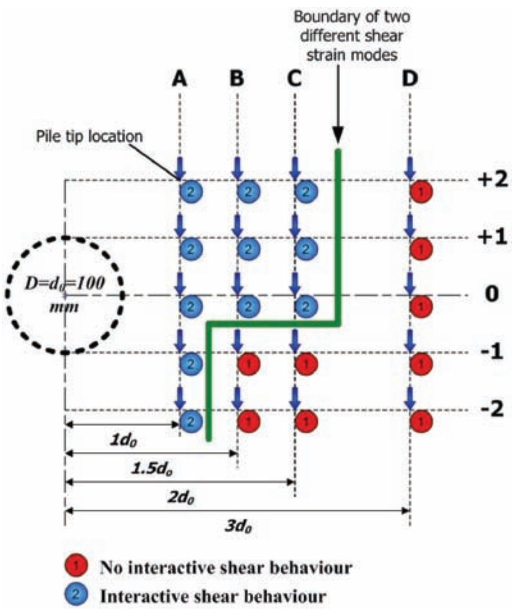


Figure 11. Boundary of two different shear strain modes according to pile tip locations.

Similar shear strain mode behaviour was observed at both small and large magnitudes of the volume loss.

While the model tests and FEA are two-dimensional, it is expected that similar behaviour would be found in real projects where the tunnelling presents a three-dimensional problem. However, the true boundary of two different shear strain modes in the latter may be different from the former tests and analyses.

## 6 CONCLUSIONS

Comparison between the physical model tests and the finite element analyses showed many successful points of agreement in terms of shear strain data. Based on the maximum shear strain data, it was observed that the shear strain modes developed are strongly dependent on the pile tip location and the magnitude of the volume loss. Through this study, it is recognized that the boundary of two different shear strain modes may be a useful guide for the tunnel planners who need to make a decision on the proper positioning of tunnel construction adjacent to a row of loaded piles in urban areas.

## REFERENCES


Britto, A.M. & Gunn, M.J. 1987. *Critical state soil mechanics via finite elements.* Chichester, UK: Ellis Horwood Limited.

Kwok, H.Y. & Swajani, C. 2001. *Precise measurement technique.* 3rd year project report, Department of Civil and Environmental Engineering, University College London, University of London.

Lee, Y.J. 2004. *Tunnelling adjacent to a row of loaded piles.* PhD Thesis, University College London, University of London.

Lee, Y.J. & Bassett, R.H. 2006. Application of a photogrammetric technique to a model tunnel. *Tunnelling and Underground Space Technology* 21(1): 79–96.

Woodhouse, N.G. 2000. *Geometric models appropriate for engineering analysis from vision metrology data.* PhD thesis, University College London, University of London.

Woodhouse, N.G., Robson, S. & Eyre, J.R. 1999. Vision metrology and three dimensional visualisation in structural testing and monitoring. *Photogrammetric Record* 16(94): 625–641.

Woods, R. & Rahim, A. 2001. *SAGE-CRISP Technical Manual, Version 4.* The CRISP Consortium Ltd. http://www.mycrisp.com/demo/TECHMAN.pdf

Yamamoto, K. & Kusuda, K. 2001. Failure mechanisms and bearing capacities of reinforced foundations. *Geotextiles and Geomembranes* 19(3): 127–162.